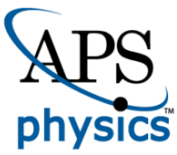

Antiferromagnetic insulators with tunable magnon-polaron Chern numbers induced by in-plane optical phonons

Bowen Ma and Gregory A. Fiete

Phys. Rev. B **105**, L100402 — Published 3 March 2022

DOI: 10.1103/PhysRevB.105.L100402

Antiferromagnetic Insulators with Tunable Magnon-Polaron Chern Numbers Induced by In-plane Optical Phonons

Bowen Ma[1, 2, 3] and Gregory A. Fiete[4, 5]

[1] *Department of Physics, The University of Texas at Austin, Austin, Texas 78712, USA*
[2] *Department of Physics, The University of Hong Kong, Hong Kong, China*
[3] *HKU-UCAS Joint Institute of Theoretical and Computational Physics at Hong Kong, Hong Kong, China*
[4] *Department of Physics, Northeastern University, Boston, Massachusetts 02115, USA*
[5] *Department of Physics, Massachusetts Institute of Technology, Cambridge, Massachusetts 02139, USA*

(Dated: February 22, 2022)

We theoretically study magnon-phonon hybrid excitations (magnon-polarons) in two-dimensional antiferromagnets on a honeycomb lattice. With an in-plane Dzyaloshinskii-Moriya interaction (DMI) allowed from mirror symmetry breaking from phonons, we find non-trivial Berry curvature around the anti-crossing rings among magnon and both optical and acoustic phonon bands, which gives rise to finite Chern numbers. We show that the Chern numbers of the magnon-polaron bands can be manipulated by changing the magnetic field direction or strength. We evaluate the thermal Hall conductivity reflecting the non-trivial Berry curvatures of magnon-polarons and propose a valley Hall effect resulting from spin-induced chiral phonons as a possible experimental signature. Our study complements prior work on magnon-phonon hybridized systems without optical phonons and suggests possible applications in spin caloritronics with topological magnons and chiral phonons.

Introduction. Antiferromagnetic materials have recently attracted a great deal of attention within the community of spintronics [1–3], because they are rather insensitive to the perturbation of magnetic fields and have small stray fields with fast THz magnetic dynamics compared to ferromagnets with frequencies in the GHz range. Research over the past decade has focused on spin dynamics and spin transport in antiferromagnets, which may originate from spin-transfer torques [4, 5], domain-wall motion [6], and the spin Seebeck effect [7–9]. Magnons, as collective excitations emerging from magnetic order, have low-dissipation and permit a pure spin transport without Joule heating, leading to a surge of interest in utilizing magnons for spintronics. Many magnonic analogs of electronic phenomena, such as the magnon thermal Hall effect [10–12], the magnon Nernst effect [13–15] and the magnonic Edelstein effect [16, 17], have been theoretically studied and experimentally observed.

Along with magnonics, there is also a potential application in spintronics by combining magnetic orders with non-trivial band topology [18]. Topologically protected states are usually robust and only weakly affected by disorders. They can provide a high charge-to-spin conversion efficiency [19], exhibit strong magnetoresistance [20, 21] and possess a number of exotic phenomena such as the quantum anomalous Hall effect [22, 23] and chiral Majorana fermions [24]. In addition to fermionic topological excitations, there is also an emerging field of investigating topological bosonic excitations, such as topological magnons [25–28] and topological phonons [29–31]. Moreover, some recent works have shown topological properties in hybridized systems between magnons and acoustic phonons with the magnetoelastic coupling [32–34], the Dzyaloshinskii-Moriya interaction (DMI) [35, 36], and the dipolar coupling [37]. However, a study of the coupling between magnons and optical phonons is still lacking.

In this Letter, we study hybrid magnon-phonon excitations in a 2D collinear antiferromagnetic insulator (AFI) on the honeycomb lattice. The topological magnon bands originate from an in-plane nearest-neighbor DMI permitted by mirror symmetry breaking [38–40], which can be generically achieved in 2D van der Waals heterostructures, in the presence of magnon-phonon coupling. Since van der Waals antiferromagnets naturally possess at least two sublattices, it is possible to realize the coupling between magnons and optical phonons. In such a coupled magnon-(optical) phonon system, which has not been studied in the ferromagnetic case [35], we find non-zero Chern numbers with finite Berry curvatures and chiral phonons at high symmetry points [52, 53].

We also show that the Chern numbers of magnon-polaron bands and the phonon chiralities can be manipulated by an external magnetic field. For connection to experiments, we evaluate the thermal Hall conductivity and propose a spin-induced valley Hall effect [53] as a possible experimental observation. We emphasize that our results are generic to many lattice structures and can be easily generalized to three-dimensional systems, as discussed at the end of this Letter. Our work suggests antiferromagnets with multiple sublatticesin contrast to ferromagnetsserve as promising platforms to realize tunable topological excitations hybridizing magnons with both acoustic and optical phonons, where the topology of the bands can provide robust information transport and may find possible applications in spintronics.

Model. We consider a system with collinear AFI Neel order on a honeycomb lattice, where the magnetic moments are perpendicular to the plane, i.e., $\mathbf{S}_{A,B} = \pm S\hat{\mathbf{z}}$

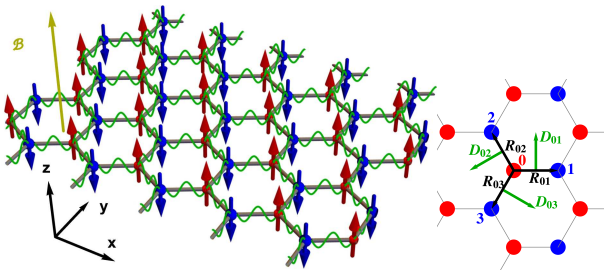

(a) (b)

FIG. 1. (Color online.) (a) Schematic illustration of a hybrid magnon-phonon system. The ground state of the magnetization is Neel order along the z-axis (red and blue arrows, color denoting the A and B sublattices). (b) DM vectors (green arrows) for the nearest bonds originated from mirror symmetry $\mathcal{M}_{yz}$ breaking.

for the A and B sublattices respectively [see Fig. 1(a)]. The Hamiltonian describing both spin and lattice degree of freedom can be written as $H = H_m + H_p + H_{mp}$, where the magnetic part H_m is given by,

$$H_m = J_1 \sum_{\langle ij \rangle} \mathbf{S}_i \cdot \mathbf{S}_j - J_2 \sum_{\langle\langle ij \rangle\rangle} \mathbf{S}_i \cdot \mathbf{S}_j - \frac{K_z}{2} \sum_i (S_i^z)^2 - \mathcal{B} \sum_i S_i^z, \tag{1}$$

where J_1 (J_2) > 0 is the (next-)nearest-neighbor antiferromagnetic (ferromagnetic) Heisenberg exchange coupling, $K_z > 0$ is the easy-axis anisotropy and $\mathcal{B} = g\mu_B B$ is the external effective Zeeman magnetic field. The phonon part H_p can be expressed as,

$$H_p = \sum_i \frac{\mathbf{p}_i^2}{2M_i} + \frac{k_1}{2} \sum_{\langle ij \rangle} (\hat{\mathbf{R}}_{ij}^0 \cdot \mathbf{u}_{ij})^2 + \frac{k_2}{2} \sum_{\langle\langle ij \rangle\rangle} (\hat{\mathbf{R}}_{ij}^0 \cdot \mathbf{u}_{ij})^2, \tag{2}$$

where $\mathbf{u}_{ij} = \mathbf{u}_j - \mathbf{u}_i$ is the in-plane displacement of the lattice, $\hat{\mathbf{R}}_{ij}^0$ is the unit vector along bond ij in equilibrium, and k_1 (k_2) is the spring constant that corresponds to the elastic energy between two (next) nearest neighbor ions. Here we ignore out-of-plane vibrations as they are higher-order terms [41].

For the magnon-phonon coupling H_{mp}, we begin from an in-plane nearest-neighbor DMI originating from mirror symmetry breaking. By Moriya's rule [42, 43], the direction of the DM vectors is perpendicular to the bond, i.e., $\mathbf{D}_{ij} \propto \hat{\mathbf{z}} \times \mathbf{R}_{ij}$ [see Fig. 1(b)]. The DMI Hamiltonian is then

$$H_D = \mathbf{D}_{ij} \cdot (\mathbf{S}_i \times \mathbf{S}_j). \tag{3}$$

This term is not included in Eq. (1) since it is well-known that DM vectors perpendicular to spin moments do not appear in the linear spin-wave Hamiltonian [10, 35, 36] and we assume it does not appreciably change (i.e., the change is numerically small) the Neel ground state order as long as the exchange coupling and anisotropy is large enough. However, both the magnitude and direction of $\mathbf{D}_{ij}$ depend on $\mathbf{R}_{ij}$ and thus it couples lattice and spin degrees of freedom. To lowest order of $\mathbf{u}_{ij}$ and $\delta\mathbf{s}_i = \mathbf{S}_i - \langle \mathbf{S}_i \rangle$, Eq. (3) can be expanded in a partial mean-field form as [41],

$$\begin{aligned} H_{mp} &\approx \frac{DS}{a} \sum_{\langle ij \rangle} \mathbf{u}_{ij} \left[\mathcal{I}_2 - \hat{\mathbf{R}}_{ij}^0 \hat{\mathbf{R}}_{ij}^0 \right] (\delta\mathbf{s}_{A,i} + \delta\mathbf{s}_{B,j}) \\ &= \frac{DS}{a} \sum_{\langle ij \rangle} \left(\hat{\mathbf{R}}_{ij}^0 \times \mathbf{u}_{ij} \right) \cdot \left[\hat{\mathbf{R}}_{ij}^0 \times (\mathbf{S}_{A,i} + \mathbf{S}_{B,j}) \right], \end{aligned} \tag{4}$$

where $D = |\mathbf{D}_{ij}|$ is the magnitude of the DMI, $a = |\mathbf{R}_{ij}^0|$ is the bond length, $\mathcal{I}_2$ is the 2×2 identity matrix, $\hat{\mathbf{R}}_{ij}^0 \hat{\mathbf{R}}_{ij}^0$ is the Kronecker product between two $\hat{\mathbf{R}}_{ij}^0$'s and $\delta\mathbf{s}_{A(B),i} = (S_{A(B),i}^x,\ S_{A(B),i}^y) = \mathbf{S}_{A(B),i} - (+) S\hat{\mathbf{z}}$. The second equation mimics a Rashba-type spin-orbital coupling [44, 45] or a Raman spin-phonon interaction [30, 46–48], which has been studied in topological aspects of spin or phonon systems.

It is clear from Eq. (4) that the DMI induced magnon-phonon coupling breaks the combined symmetry of time reversal plus 180° rotation about an in-plane axis [49, 50]. With magnetic fields, this symmetry breaking allows the existence of a thermal Hall effect [51], which is absent in a magnon-only or phonon-only scenario. Moreover, in contrast to the ferromagnetic case, $H_{mp} + H_m$ also breaks inversion symmetry [13] and gives rise to chiral phonons at high symmetry points [52, 53], as will be shown below.

Band Topology. As magnons and phonons are both bosons, one can treat them equivalently as magnon-polaron excitations and re-write $H = H_m + H_p + H_{mp}$ to a generalized Bogliubov-de Gennes (BdG) form as [41],

$$H_{\mathbf{k}} = \begin{bmatrix} \frac{1}{2}\tilde{H}_m(\mathbf{k}) & \tilde{H}_{mp}(\mathbf{k}) & 0 \\ \tilde{H}_{mp}^\dagger(\mathbf{k}) & \frac{1}{2}D(\mathbf{k}) & 0 \\ 0 & 0 & \frac{\mathcal{I}_4}{2M} \end{bmatrix}, \tag{5}$$

with representation $\mathbf{X}_{\mathbf{k}} = \left(a_{\mathbf{k}}, b_{\mathbf{k}}, a_{-\mathbf{k}}^\dagger, b_{-\mathbf{k}}^\dagger, \mathbf{u}_{\mathbf{k}}, \mathbf{p}_{-\mathbf{k}} \right)^T$, where $a_{\mathbf{k}}$ ($b_{\mathbf{k}}$) is the A (B) sublattice magnon annihilation operator in a Holstein-Primakoff representation [54], S_A^+ (S_B^+) $= \sqrt{2S}a$ ($b^\dagger$), $\mathbf{u}_{\mathbf{k}}$ ($\mathbf{p}_{-\mathbf{k}}$) is a four-vector for two-dimensional displacements (momenta) of A and B sublattices, $\tilde{H}_m$ ($\mathbf{k}$) ($\tilde{H}_{mp}(\mathbf{k})$) corresponds to Eq. (1) [Eq. (4)] and $D(\mathbf{k})$ is the dynamical matrix corresponding to Eq. (2). Under this representation, the bosonic commutator is written as

$$\left[\mathbf{X}_{\mathbf{k}},\ \mathbf{X}_{\mathbf{k}}^\dagger \right] = g = \begin{bmatrix} \mathcal{I}_2 & & & \\ & -\mathcal{I}_2 & & \\ & & & i\mathcal{I}_4 \\ & & -i\mathcal{I}_4 & \end{bmatrix}, \tag{6}$$

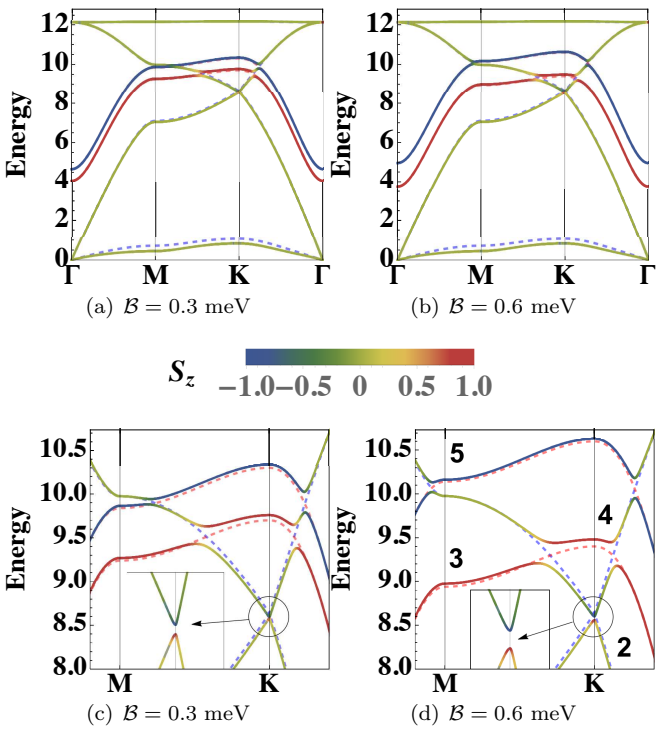

(a) $\mathcal{B} = 0.3$ meV (b) $\mathcal{B} = 0.6$ meV (c) $\mathcal{B} = 0.3$ meV (d) $\mathcal{B} = 0.6$ meV

FIG. 2. (Color online.) Topological magnon-polaron bands. Energy is in meV. We set parameters as $S = 3/2$, $J_1 = 2.0$ meV, $J_2 = 0.0$ meV, $K_z = 1.0$ meV, $m_B/m_A = 1$, $\hbar\sqrt{k_1/m_A} = 7.0$ meV, $\hbar\sqrt{k_2/m_A} = 0.5$ meV, $D = 0.2$ meV. The blue (red) dashed lines are phonon (magnon) dispersions without DMI. The solid lines are magnon-polaron bands with DMI, where the color shows the z-component angular momentum, indicating whether the hybridization is more "magnonic" (as blue for $S_z = -1$ or red for $S_z = +1$) or "phononic" (as green for $S_z = 0$). (a)(b) Full band dispersions along high symmetry path. (c)(d) Bands around anti-crossing points. Band numbering is shown in (d). The insets show the gap opens at **K** and allows phonons with different chiralities (red or blue). Details are shown in Fig. 4.

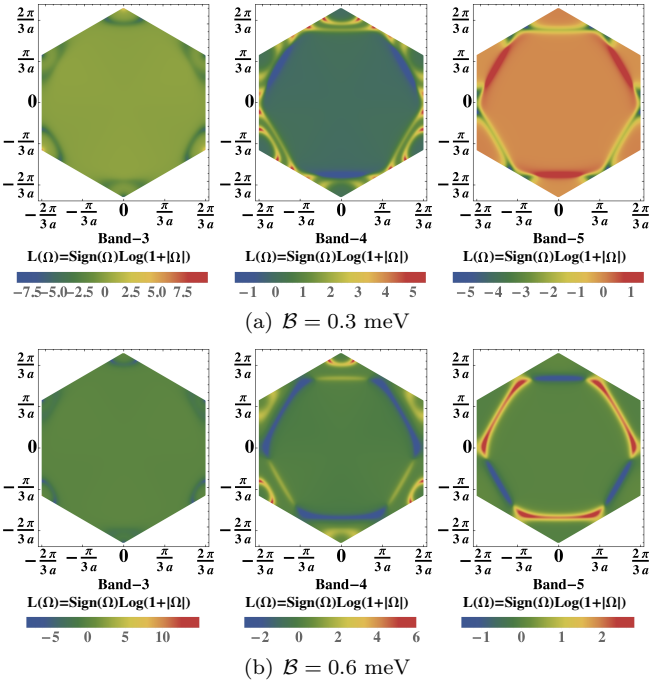

(a) $\mathcal{B} = 0.3$ meV (b) $\mathcal{B} = 0.6$ meV

FIG. 3. (Color online.) Berry curvatures of the middle three anti-crossed bands in Fig. 2. Band numbers are ordered from bottom to top. When the magnetic field increases, there is one gapped ring around **Γ** between band 3 and 4 splits into two rings around **K** and **K′** leading to a topological phase transition.

and the eigenstates satisfy [55, 56],

$$gH_{\mathbf{k}}\left|\psi_{n\mathbf{k}}\right\rangle = \sigma_{nn}E_{n\mathbf{k}}\left|\psi_{n\mathbf{k}}\right\rangle,\ \left\langle\psi_{n\mathbf{k}}\right|g\left|\psi_{n'\mathbf{k}}\right\rangle = \sigma_{nn'}, \quad (7)$$

where $\sigma = \sigma_z \bigotimes \mathcal{I}_{6\times6}$ stands for particle-hole space. With particle-hole symmetry, $E_{n\mathbf{k}} = E_{n+6,-\mathbf{k}}$ and thus we only plot the first six eigenvalues in Fig. 2 and others are redundant. Here $S_z = \left\langle\psi^R_{n\mathbf{k}}\right|\left(-a^\dagger_{\mathbf{k}}a_{\mathbf{k}} + b^\dagger_{\mathbf{k}}b_{\mathbf{k}} + \mathbf{u}^A_{\mathbf{k}}\times\mathbf{p}^A_{-\mathbf{k}} + \mathbf{u}^B_{\mathbf{k}}\times\mathbf{p}^B_{-\mathbf{k}}\right)\left|\psi^R_{n\mathbf{k}}\right\rangle$ mediates both magnon spins and phonon polarizations [52].

In Fig. 2, there are gapped rings around **Γ** or **K** (**K′**) formed by anti-crossing points among magnon and phonon bands due to the DMI coupling, which gives rise to nontrivial topological properties in this magnon-polaron system. In such a generalized BdG system, the Berry curvature is given by the Bloch wavefunction $\left|u_{n\mathbf{k}}\right\rangle = e^{-i\mathbf{k}\cdot\mathbf{r}}\left|\psi_{n\mathbf{k}}\right\rangle$ as [12, 41] $\mathbf{\Omega}_{n\mathbf{k}} = i\left\langle\nabla_{\mathbf{k}}u_{n\mathbf{k}}\right|g\times\left|\nabla_{\mathbf{k}}u_{n\mathbf{k}}\right\rangle$, and the Chern numbers can be obtained by integrating Berry curvature $\Omega^z_{n\mathbf{k}}$ along the Brillouin zone as [57] $C_n = \frac{1}{2\pi}\int_{BZ} d^2\mathbf{k}\ \Omega^z_{n\mathbf{k}}$, from which we calculate the band Chern numbers [since the top (also bottom) two bands are degenerate at **Γ** point, we add up the Berry curvature of the two bands to obtain a well-defined Chern number] by the Fukui method [41, 58] and find that the magnetic field can change the Chern numbers by integers.

In Fig. 2(a), the Chern numbers for the middle three anti-crossed bands from low to high are $(-2, +4, -2)$, while they change to $(-2, +1, +1)$ in Fig. 2(b) by a phase transition when $\mathcal{B} > \mathcal{B}_c(\approx 0.41$ meV with the parameters in Fig. 2 [41]). Since in this parameter region the coupling barely affects acoustic modes and the longitudinal optical (LO) mode, the band topology can be effectively mapped into an SU(3) algebra [34, 59]. Here, instead of an analytic calculation (which is generally not accessible), we achieve an understanding of the band topology more intuitively by looking at Berry curvatures.

As shown in Fig. 3, non-trivial Berry curvatures are induced around the anti-crossing regions, and thus the change of Chern numbers can be intuitively understood as a pair of gapped rings around **K** and **K′** combining into or split by one anti-crossing ring around **Γ**. Notice that there are opposite Berry curvatures at **K** and **K′** in band-3 from the gap by spin-induced inversion symmetry

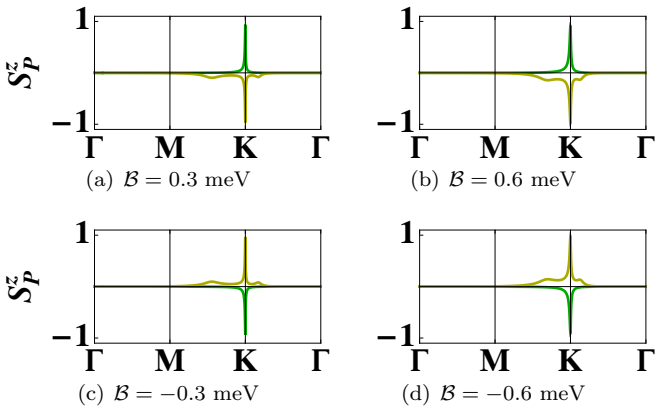

(a) $\mathcal{B} = 0.3$ meV (b) $\mathcal{B} = 0.6$ meV

(c) $\mathcal{B} = -0.3$ meV (d) $\mathcal{B} = -0.6$ meV

FIG. 4. (Color online.) Phonon polarization contribution $S_P^z = \langle \mathbf{u}_{\mathbf{k}}^A \times \mathbf{p}_{-\mathbf{k}}^A + \mathbf{u}_{\mathbf{k}}^B \times \mathbf{p}_{-\mathbf{k}}^B \rangle$ to S_z in Fig. 2. The green (yellow) line is for band 2 (band 3). The chiralities of phonons occur around **K**.

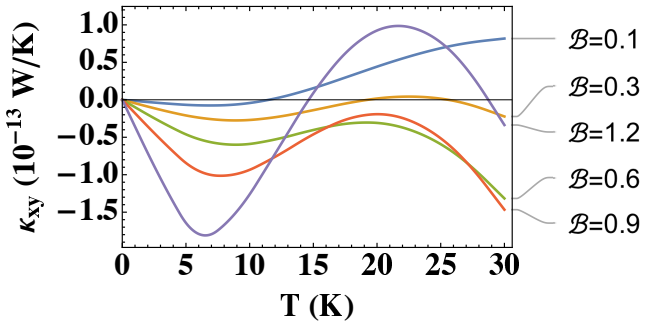

(a) Thermal Hall response. $\mathcal{B}$ is in unit of meV.

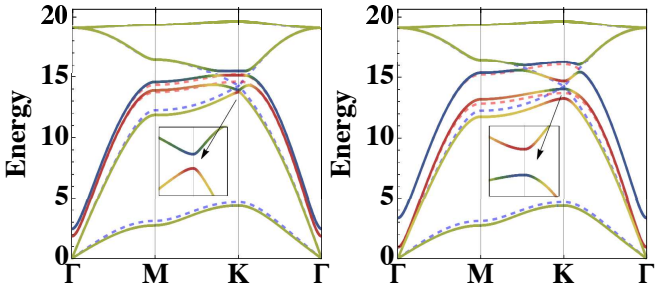

(b) $\mathcal{B} = 0.3$ meV with Chern number (0, 0, −2, +4, −2, 0). (c) $\mathcal{B} = 1.2$ meV with Chern number (0, +2, −2, +2, −2, 0).

FIG. 5. (Color online.) (a) Thermal Hall response using parameters from $MnPS_3$. (b),(c) Band structures and Chern numbers for different external fields. See main text for details.

breaking, but it does not contribute to the Chern number due to a cancellation between these two valleys [53]. However, as shown in Fig. 4(a)-(d), large phonon angular momentum $S_P^z = \langle \mathbf{u}_{\mathbf{k}}^A \times \mathbf{p}_{-\mathbf{k}}^A + \mathbf{u}_{\mathbf{k}}^B \times \mathbf{p}_{-\mathbf{k}}^B \rangle$ occurs at **K** for band 2 and 3 giving rise to chiral phonons. The polarization of these phonons can be flipped by reversing the magnetic field and they can contribute to a valley Hall effect [53].

Similar to the physics of gapped 2D Dirac systems [60], the physics of an anti-crossing magnon-phonon pair can be effectively described by

$$H_{\text{eff}} = \frac{E_{m\mathbf{k}}^{\pm} + E_{p\mathbf{k}}^{\pm}}{2}\mathcal{I}_2 + \mathbf{d}_{\mathbf{k}}^{\pm\pm} \cdot \boldsymbol{\sigma} + V_{\mathbf{k}}, \tag{8}$$

where $E_{m\mathbf{k}}^{+(-)}$ is the upper (lower) magnon energy without the DMI, $E_{p\mathbf{k}}^{+(-)}$ is the transverse optical (longitudinal acoustic) phonon energy without the DMI, $\boldsymbol{\sigma} = (\sigma_x, \sigma_y, \sigma_z)$ is the Pauli matrices, $\mathbf{d}_{\mathbf{k}}^{\pm\pm}$ opens a gap between $E_{m\mathbf{k}}^{\pm}$ and $E_{p\mathbf{k}}^{\pm}$ arising from the DMI and can be regarded as an analog of the gaping term in the Kane-Mele model [61, 62], and $V_{\mathbf{k}}$ includes terms that do not conserve particle numbers and perturbations that do not participate in opening the gap between the two bands [33, 34]. A Skyrmion (anti-Skyrmion) topological charge Q $(-Q)$ can then be defined with $\mathbf{d}_{\mathbf{k}}^{\pm\pm}$ as $Q = \frac{1}{4\pi}\int d^2\mathbf{k}\, \hat{\mathbf{d}}_{\mathbf{k}} \cdot \left(\partial_{k_x}\hat{\mathbf{d}}_{\mathbf{k}} \times \partial_{k_y}\hat{\mathbf{d}}_{\mathbf{k}}\right)$ for the upper (lower) band. In general, the analytical expression for $\mathbf{d}_{\mathbf{k}}^{\pm\pm}$ is not available, but since $\mathbf{d}_z^{\pm\pm} = (E_{m\mathbf{k}}^{\pm} - E_{p\mathbf{k}}^{\pm})/2$, the Skyrmion numbers will change with the moving of anti-crossing rings [33]. As the band Chern number reflects the winding number of $\hat{\mathbf{d}}_{\mathbf{k}}$ wrapping the unit sphere in the Brillouin zone, a skyrmion arising from $\mathbf{d}$ with charge Q determines the lower (upper) band with a Chern number Q $(-Q)$ [63]. In addition to changing the field strength, reversing the external field will also change the Chern numbers by flipping the sign, thus we find the topology of our system is highly tunable.

Thermal and Valley Hall effects. In order to connect our results with possible experimental observations, we evaluate the thermal Hall effect rising from the nontrivial Berry curvature of magnon-polaron bands. With a longitudinal temperature gradient $\nabla_y T$, an anomalous transverse motion of magnon-polaron excitations can be induced by the fictitious field $\Omega_{n\mathbf{k}}^z$ associated with a transverse thermal conductivity κ_{xy} as [12]

$$\kappa_{xy} = -\frac{k_B^2 T}{\hbar V}\sum_{n,\mathbf{k}}\left[c_2(g(E_{n\mathbf{k}})) - \frac{\pi^2}{3}\right]\Omega_{n\mathbf{k}}^z, \tag{9}$$

where $c_2(x) = (1+x)\ln^2(1+1/x) - \ln^2 x - 2\text{Li}_2(-x)$, $\text{Li}_2(x)$ is the polylogarithm function, and $g(x) = (\exp(x/k_BT) - 1)^{-1}$ is the Bose-Einstein distribution.

In Fig. 5, we evaluate κ_{xy} with parameters [64–66] for $MnPS_3$ as $m_A = m_B = M = 55$ u, $S = 5/2$, $J_1 = 1.54$ meV, $J_2 = 0.14$ meV, $g = -2.0$ and set $K_z = 0.1$ meV, $D = 0.5$ meV, $\hbar\sqrt{k_1/M} = 11$ meV and $\hbar\sqrt{k_2/M} = 2.2$ meV. At the low field, the two magnon bands couple with the transverse optical (TO) phonon giving a Chern number distribution (0, +2, −4, +2) from bottom to top, while they couple with the TO and longitudinal acoustic (LA) phonon respectively at high field giving a Chern distribution (−2, +2, −2, +2). These results are also consistent with our analysis on band topology by look-

ing at the moving of gapped rings. The change of κ_{xy} with magnetic field results from the topological transition with different Chern numbers, while the sign change with temperature reflects the competition among bands of different Chern numbers which come to dominate the transverse thermal transport.

In addition, as the spatial inversion symmetry is broken by the spin degree of freedom, the gap opens at $\mathbf{K}$ and $\mathbf{K}'$ valley, and thus gives rise to chiral phonons with different polarizations at these high symmetry points [see Fig. 2(c)(d) and 5(b)(c)]. This has not been discussed in previous studies in coupled systems without optical phonons. By introducing a longitudinal strain gradient across the system, we expect opposite motion of chiral phonons at different valleys since $v \propto -\mathbf{E}_{\text{strain}} \times \mathbf{\Omega}$ in the transverse direction which creates a temperature difference between two edges [53]. The sign of the valley Hall signal is also controllable by flipping the external magnetic field. As these two Hall effects originate from the non-trivial topology of the system, we expect to observe a thermal Hall signal only weakly affected by the bulk disorder.

Discussion. In this Letter, we study the topology of magnon-polaron bands in a 2D honeycomb Neel order antiferromagnet with an in-plane DMI induced by magnon-phonon coupling. Without the DMI, the magnon or phonon bands are trivial, while non-trivial Berry curvature occurs around the anti-crossing rings opened by the magnon-phonon coupling. In contrast to previous studies on ferromagnetic magnons or on magnons coupled with only acoustic phonons, in our case, antiferromagnetic magnons can couple with both optical and acoustic phonons giving rise to two remarkable resultshighly tunable integer Chern numbers with an external magnetic field and the existence of chiral phonons. We also investigated a field-tunable thermal Hall effect induced from the finite Berry curvatures and proposed valley Hall effects by spin-induced chiral phonons, both of which will generate significant experimental interests in the community.

Even though we study the model on a honeycomb lattice, the coupling can be expressed with a displacement field $\mathbf{u} \approx \mathbf{u}_{ij}/a$ and a staggered spin field $\mathbf{n} \approx (\mathbf{S}_A - \mathbf{S}_B)/2S$ as $\frac{DS^2}{a^3}(\nabla \times \mathbf{u}) \cdot (\nabla \times \mathbf{n})$ from Eq. (4), which does not depend on lattice details [41]. This is similar to Rashba spin-orbital coupling and Raman spin-phonon interaction, revealing the underlying topological nature of this hybridized system. We believe this universal form is the key to the topology and gives a crucial insight that will be of interest to a broad community of researchers studying the consequences of magnon-phonon interactions. This 2D model can also be generalized to a 3D system with mirror symmetry breaking in the bulk [67, 68] and it can couple the magnons with out-of-plane phonon modes as well which could further enrich the physics of topology. In principle, our method can be used in any bosonic system such as plasmonics [69, 70] and photonics [71], and may find similar and interesting applications there. To our best knowledge, this is the first study on the field-tunable topological properties and phonon chiralities arising from the coupling between antiferromagnetic magnons and optical phonons. Our work opens a new avenue in the study of hybridized magnon-phonon excitations by treating the optical and acoustic phonons on equal footing, and it may be useful to design tunable transport devices in the field of spintronics and draws a connection to chiral phonons with spin caloritronics.

Acknowledge. We thank Nemin Wei and Naichao Hu for helpful discussions on band topology. We gratefully acknowledge support from NSF DMR-1949701 and NSF DMR-2114825, with additional support from the NSF through the Center for Dynamics and Control of Materials: an NSF MRSEC under Cooperative Agreement No. DMR-1720595. This work was performed in part at the Aspen Center for Physics, which is supported by National Science Foundation grant PHY-1607611.

[1] T. Jungwirth, X. Marti, P. Wadley, and J. Wunderlich, Nature nanotechnology **11**, 231 (2016).
[2] T. Jungwirth, J. Sinova, A. Manchon, X. Marti, J. Wunderlich, and C. Felser, Nature Physics **14**, 200 (2018).
[3] V. Baltz, A. Manchon, M. Tsoi, T. Moriyama, T. Ono, and Y. Tserkovnyak, Reviews of Modern Physics **90**, 015005 (2018).
[4] R. Cheng, J. Xiao, Q. Niu, and A. Brataas, Physical review letters **113**, 057601 (2014).
[5] H. V. Gomonayand V. M. Loktev, Physical Review B **81**, 144427 (2010).
[6] O. Gomonay, T. Jungwirth, and J. Sinova, arXiv preprint arXiv:1602.06766 (2016).
[7] S. M. Wu, W. Zhang, K. Amit, P. Borisov, J. E. Pearson, J. S. Jiang, D. Lederman, A. Hoffmann, and A. Bhattacharya, Physical review letters **116**, 097204 (2016).
[8] Y. Ohnuma, H. Adachi, E. Saitoh, and S. Maekawa, Physical Review B **87**, 014423 (2013).
[9] S. Rezende, R. Rodríguez-Suárez, and A. Azevedo, Physical Review B **93**, 014425 (2016).
[10] H. Katsura, N. Nagaosa, and P. A. Lee, Physical review letters **104**, 066403 (2010).
[11] Y. Onose, T. Ideue, H. Katsura, Y. Shiomi, N. Nagaosa, and Y. Tokura, Science **329**, 297 (2010).
[12] R. Matsumotoand S. Murakami, Physical Review B **84**, 184406 (2011).
[13] R. Cheng, S. Okamoto, and D. Xiao, Physical review letters **117**, 217202 (2016).
[14] V. A. Zyuzinand A. A. Kovalev, Physical review letters **117**, 217203 (2016).
[15] Y. Shiomi, R. Takashima, and E. Saitoh, Physical Review B **96**, 134425 (2017).

[16] B. Li, A. Mook, A. Raeliarijaona, and A. A. Kovalev, Physical Review B **101**, 024427 (2020).
[17] H. Zhangand R. Cheng, Applied Physics Letters **117**, 222402 (2020).
[18] L. Šmejkal, Y. Mokrousov, B. Yan, and A. H. MacDonald, Nature physics **14**, 242 (2018).
[19] H. Wang, J. Kally, J. S. Lee, T. Liu, H. Chang, D. R. Hickey, K. A. Mkhoyan, M. Wu, A. Richardella, and N. Samarth, Physical review letters **117**, 076601 (2016).
[20] X. Wang, Y. Du, S. Dou, and C. Zhang, Physical Review Letters **108**, 266806 (2012).
[21] T. Liang, Q. Gibson, M. N. Ali, M. Liu, R. Cava, and N. Ong, Nature materials **14**, 280 (2015).
[22] C.-Z. Chang, J. Zhang, X. Feng, J. Shen, Z. Zhang, M. Guo, K. Li, Y. Ou, P. Wei, L.-L. Wang, *et al.*, Science **340**, 167 (2013).
[23] Y. Deng, Y. Yu, M. Z. Shi, Z. Guo, Z. Xu, J. Wang, X. H. Chen, and Y. Zhang, Science **367**, 895 (2020).
[24] Q. L. He, L. Pan, A. L. Stern, E. C. Burks, X. Che, G. Yin, J. Wang, B. Lian, Q. Zhou, E. S. Choi, *et al.*, Science **357**, 294 (2017).
[25] L. Zhang, J. Ren, J.-S. Wang, and B. Li, Physical Review B **87**, 144101 (2013).
[26] A. Mook, J. Henk, and I. Mertig, Physical Review B **90**, 024412 (2014).
[27] R. Chisnell, J. Helton, D. Freedman, D. Singh, R. Bewley, D. Nocera, and Y. Lee, Physical review letters **115**, 147201 (2015).
[28] F.-Y. Li, Y.-D. Li, Y. B. Kim, L. Balents, Y. Yu, and G. Chen, Nature communications **7**, 1 (2016).
[29] E. Prodanand C. Prodan, Physical review letters **103**, 248101 (2009).
[30] L. Zhang, J. Ren, J.-S. Wang, and B. Li, Physical review letters **105**, 225901 (2010).
[31] Y. Jin, R. Wang, and H. Xu, Nano letters **18**, 7755 (2018).
[32] S. Parkand B.-J. Yang, Physical Review B **99**, 174435 (2019).
[33] G. Go, S. K. Kim, and K.-J. Lee, Physical review letters **123**, 237207 (2019).
[34] S. Zhang, G. Go, K.-J. Lee, and S. K. Kim, Physical review letters **124**, 147204 (2020).
[35] X. Zhang, Y. Zhang, S. Okamoto, and D. Xiao, Physical review letters **123**, 167202 (2019).
[36] S. Park, N. Nagaosa, and B.-J. Yang, Nano letters **20**, 2741 (2020).
[37] R. Takahashiand N. Nagaosa, Physical review letters **117**, 217205 (2016).
[38] K. Di, V. L. Zhang, H. S. Lim, S. C. Ng, M. H. Kuok, J. Yu, J. Yoon, X. Qiu, and H. Yang, Physical review letters **114**, 047201 (2015).
[39] S. Tacchi, R. Troncoso, M. Ahlberg, G. Gubbiotti, M. Madami, J. Åkerman, and P. Landeros, Physical review letters **118**, 147201 (2017).
[40] A. Qaiumzadeh, I. A. Ado, R. A. Duine, M. Titov, and A. Brataas, Physical review letters **120**, 197202 (2018).
[41] See supplementary materials for details on model derivations and numerical method.
[42] T. Moriya, Physical review **120**, 91 (1960).
[43] T. Moriya, Physical Review Letters **4**, 228 (1960).
[44] Y. A. Bychkov, JETP lett. **39**, 78 (1984).
[45] A. Manchon, H. C. Koo, J. Nitta, S. Frolov, and R. Duine, Nature materials **14**, 871 (2015).
[46] L. Sheng, D. Sheng, and C. Ting, Physical review letters **96**, 155901 (2006).
[47] Y. Kaganand L. Maksimov, Physical review letters **100**, 145902 (2008).
[48] J.-S. Wangand L. Zhang, Physical Review B **80**, 012301 (2009).
[49] H. Chen, Q. Niu, and A. H. MacDonald, Physical review letters **112**, 017205 (2014).
[50] M.-T. Suzuki, T. Koretsune, M. Ochi, and R. Arita, Physical Review B **95**, 094406 (2017).
[51] A. Mook, J. Henk, and I. Mertig, Physical Review B **99**, 014427 (2019).
[52] L. Zhangand Q. Niu, Physical Review Letters **112**, 085503 (2014).
[53] L. Zhangand Q. Niu, Physical review letters **115**, 115502 (2015).
[54] T. Holsteinand H. Primakoff, Physical Review **58**, 1098 (1940).
[55] A. G. Del Maestroand M. J. Gingras, Journal of Physics: Condensed Matter **16**, 3339 (2004).
[56] R. Shindou, R. Matsumoto, S. Murakami, and J.-i. Ohe, Physical Review B **87**, 174427 (2013).
[57] X.-L. Qi, T. L. Hughes, and S.-C. Zhang, Physical Review B **78**, 195424 (2008).
[58] T. Fukui, Y. Hatsugai, and H. Suzuki, Journal of the Physical Society of Japan **74**, 1674 (2005).
[59] R. Barnett, G. R. Boyd, and V. Galitski, Physical review letters **109**, 235308 (2012).
[60] B. A. Bernevig, T. L. Hughes, and S.-C. Zhang, science **314**, 1757 (2006).
[61] C. L. Kaneand E. J. Mele, Physical review letters **95**, 226801 (2005).
[62] S. K. Kim, H. Ochoa, R. Zarzuela, and Y. Tserkovnyak, Physical review letters **117**, 227201 (2016).
[63] B. A. Bernevig, *Topological insulators and topological superconductors* (Princeton university press, 2013).
[64] A. Wildes, B. Roessli, B. Lebech, and K. Godfrey, Journal of Physics: Condensed Matter **10**, 6417 (1998).
[65] P. Joyand S. Vasudevan, Physical Review B **46**, 5425 (1992).
[66] A. Hashemi, H.-P. Komsa, M. Puska, and A. V. Krasheninnikov, The Journal of Physical Chemistry C **121**, 27207 (2017).
[67] D.-H. Kim, M. Haruta, H.-W. Ko, G. Go, H.-J. Park, T. Nishimura, D.-Y. Kim, T. Okuno, Y. Hirata, Y. Futakawa, *et al.*, Nature materials **18**, 685 (2019).
[68] A. Fernández-Pacheco, E. Vedmedenko, F. Ummelen, R. Mansell, D. Petit, and R. P. Cowburn, Nature materials **18**, 679 (2019).
[69] I. Appelbaum, H. Drew, and M. Fuhrer, Applied Physics Letters **98**, 023103 (2011).
[70] P. Di Pietro, M. Ortolani, O. Limaj, A. Di Gaspare, V. Giliberti, F. Giorgianni, M. Brahlek, N. Bansal, N. Koirala, S. Oh, *et al.*, Nature nanotechnology **8**, 556 (2013).
[71] T. Ozawa, H. M. Price, A. Amo, N. Goldman, M. Hafezi, L. Lu, M. C. Rechtsman, D. Schuster, J. Simon, O. Zilberberg, *et al.*, Reviews of Modern Physics **91**, 015006 (2019).